# Effect of Na Environment on growth rate of grain and nucleation of precipitate in F/M steel cladding under Sodium and Ar-gas environment at 650°C

Tae Yong Kim[a], Sang Hun Shin[b], and Ji Hyun Kim[*]
[a]*Interdisciplinary School of Mechanical and Nuclear engineering, Ulsan National Institute of Science and Technology 100 Banyeon-ri, Eonyang-eup, Ulju-gun, Ulsan 689-798, Republic of Korea*
[b]*Korea Atomic Energy Research Institute, 989-111 Daedeokdaero, Yuseong-gu, Daejeon 305-353, Republic of Korea*
[*]*Corresponding author: kimjh@unist.ac.kr*

## 1. Introduction

Ultra-long Cycle Fast Reactor (UCRF), which is forth generator reactor, is designed with long period operation for sixty years without fuel replacement [1, 2]. Since there is no refueling unlike commercial nuclear reactor and are characters of fast reactor, we should consider long-term compatibility with sodium and study about life prediction.

Ferrite/martensite steels, which are used as cladding and structure materials, have high creep strength at 600°C and good safety probability in circumstance of fast neutrons compared to austenitic stainless steel. During the design life time (30 to 60 years), the cladding and structural materials are exposed to liquid sodium and aged at the designed operation temperature. When cladding and structural materials exposed to high temperature liquid sodium, the constituents of the components dissolve and exist as various compounds. This can accelerate the dissolution of components into coolant or disrupt flow of coolant with cumulated obstacle in loop. This change can cause a degradation of mechanical strength of structure material and thermal efficiency of UCFR. Therefore, the thermochemical reaction research, on effects of liquid sodium on ferrite/martensite steel for a long time, should additionally be performed.

This research study on effects of small changes of the material characteristics, which include chemical reaction with liquid sodium environment, and growth and nucleation of precipitates by long time aging at the environment, are studied with cladding in long-period reactor. The goal of this study is to investigate growth and nucleation of precipitates of ferrite/martensite steels in liquid sodium and its effect on grain growth. There are many changes such as Cr depletion, decarburization, segregation, precipitate and oxidation, affecting into microstructural evolution of the steels [3].

In a specific procedure, the micro-structure and the surface phenomenon of ferrite/martensite steels that are exposed in liquid sodium at high temperature by using scanning electron microscope (SEM) and transmission electron microscope (TEM) have been investigated.

After investigating precipitates formed at surface on liquid sodium and Ar-gas environments, the precipitates' Gibbs free energy is calculated with enthalpy and entropy included in the precipitates. Finally, the calculated values with diffusivity of components will become reason why the phases have different tendency on the growth rate of precipitates. As analyzing the chemical composition by TEM images, the correlation is investigated with supplementary materials.

## 2. Experiments

The test material in this study is ASTM A182 Gr.92 steel, which contains approximately 9 wt. % of chromium and 2 wt. % of tungsten. Chemical composition of this material is shown in Table. 1. Tubes of Gr.92 were manufactured by hot extrusion and multiple passes of cold drawing. The tubes were normalized at 1080℃ for 6 min and tempered at 800℃ for 6 min so as to develop a tempered martensite structure.

Table I. Chemical compositions in wt. % of Gr.92 alloy [4].

| C | Si | Mn | Cr | Ni | Mo | W |
|---|---|---|---|---|---|---|
| 0.087 | 0.21 | 0.41 | 8.69 | 0.13 | 0.38 | 1.62 |
| V | Nb | Cu | N | B | P | S |
| 0.18 | 0.07 | 0.10 | 0.046 | 0.0022 | 0.012 | 0.0018 |

Gr. 92 cladding tubes were exposed to 650℃ liquid sodium for 1583h and 3095 h, respectively. As a comparative control to test the effect of sodium, other Gr. 92 cladding tubes were encapsulated in a 99.99% pure Ar environment, and then kept in a 650℃ muffle furnace for 1601h or 2973 h. In order to observe cross section of specimens, they were cut and treated with mounting. And then, specimen cross sections were polished with 0.04 μm alumina particles and etched with a mixed acid solution (93 vol. % water, 5 vol. % nitric acid and 2 vol. % fluoric acid) to observe apparent cross sections.

The final goal of this experiment is analysis of surface, inter structure and precipitation of steels. SEM was conducted for investigating the cross section of exposed specimen.

## 3. Results

Figure 1 and 2 show chromium depletion zone to a 50μm from surface as well as 40μm of oxidation regions, like island, from surface unlike Figs. 3 and 4.

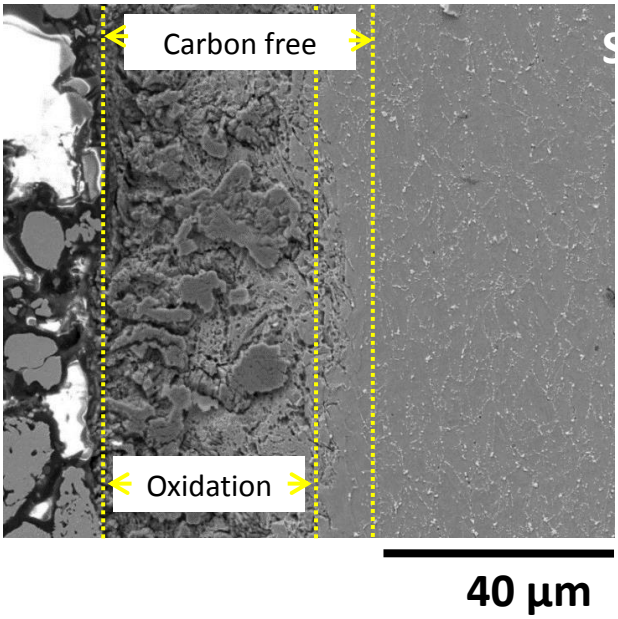


Fig. 1. SEM image of cross-section of specimen after exposure to 650℃ sodium for 1583 h [4].

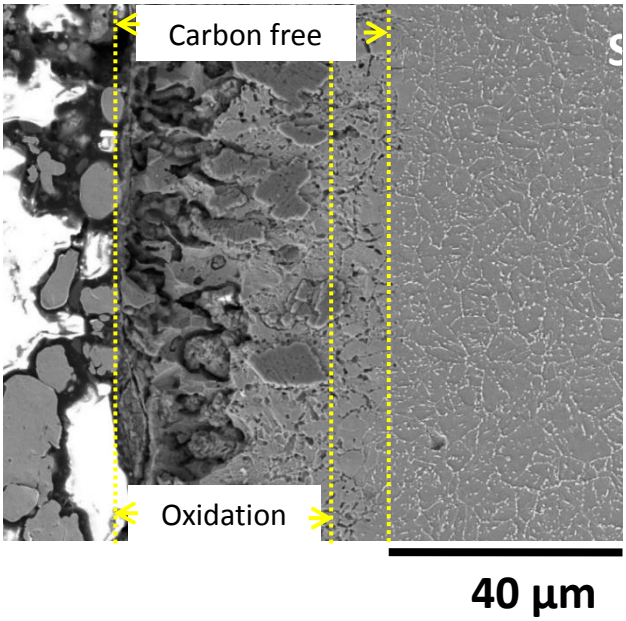


Fig. 2. SEM image of cross-section of specimen after exposure to 650℃ sodium for 3095 h [4].

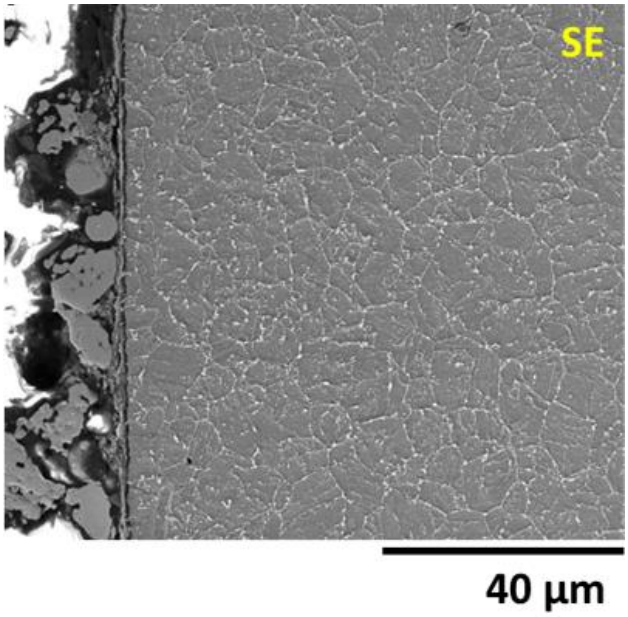


Fig. 3. SEM image of cross-section of specimen after exposure to 650℃ Ar-gas for 1601h [4].

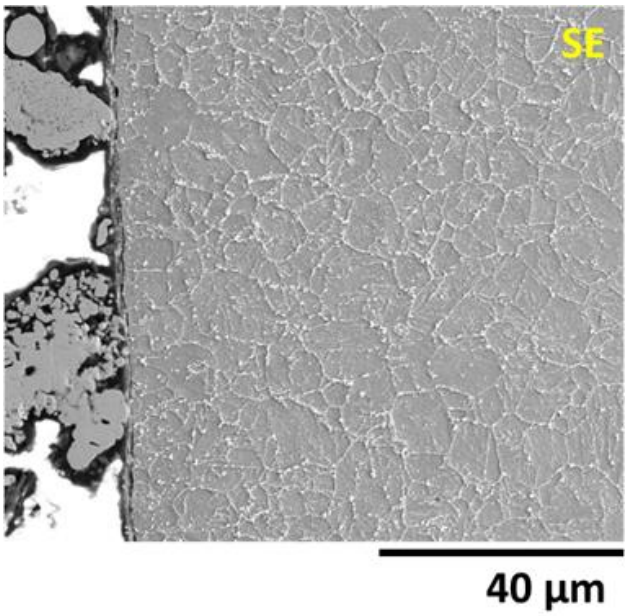


Fig. 4. SEM image of cross-section of specimen after exposure to 650℃ Ar-gas for 2973h [4].

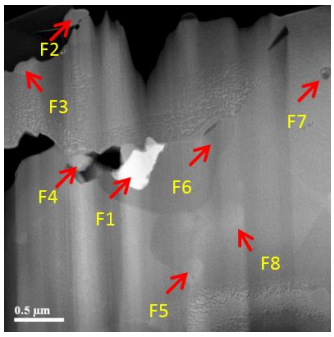


Fig. 5. TEM image of cross-section of specimen after exposure to 650℃ sodium for 1,583 h [4].

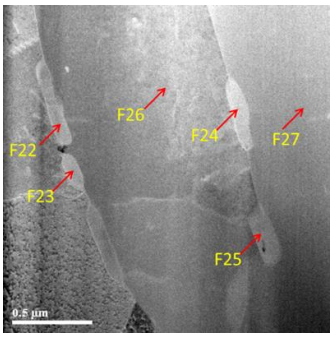


Fig. 7. TEM image of cross-section of specimen after exposure to 650℃ sodium for 3,095 h [4].

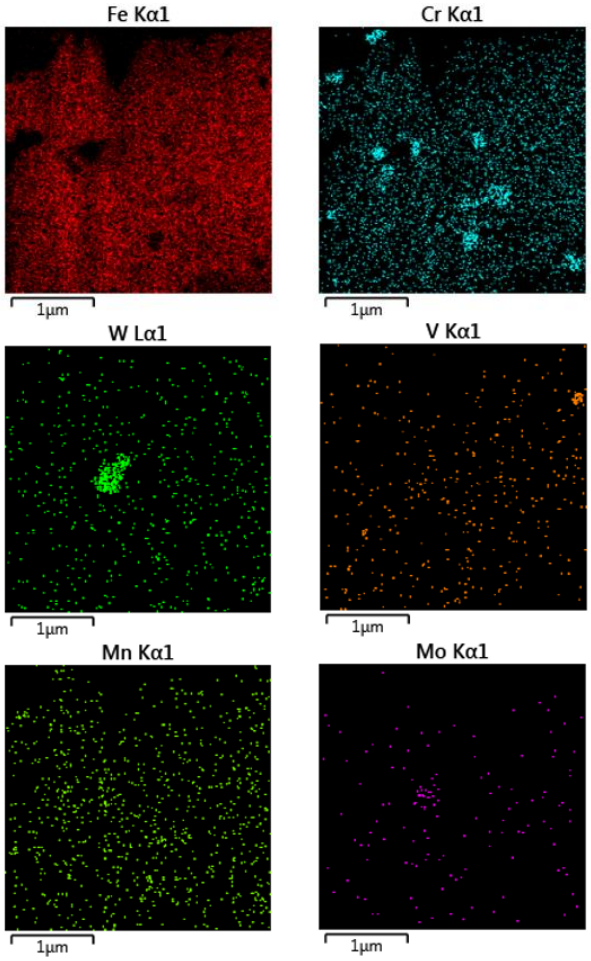


Fig. 6. EDS mapping of cross-section of specimen after exposure to 650°C sodium for 1,583 h shown in Fig. 5 [4].

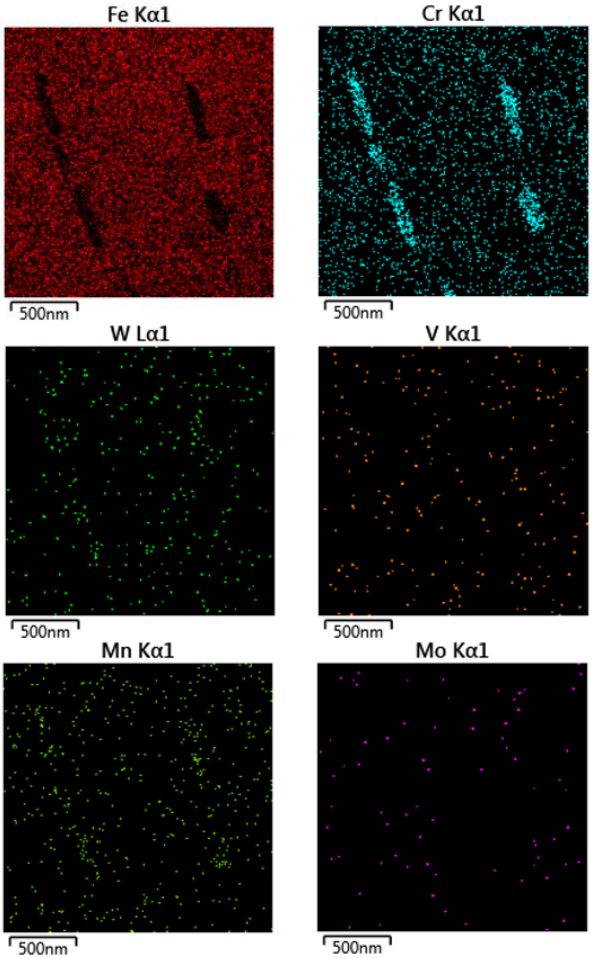


Fig. 8. EDS mapping of cross-section of specimen after exposure to 650°C sodium for 3,095 h shown in Fig. 5 [4].

Table II. Chemical composition (wt. %) of Fig. 5.

| | Fe | Cr | W | V | Mo |
|---|---|---|---|---|---|
| F1 | 53.90 | 8.83 | 28.33 | 0.13 | 8.48 |
| F2 | 30.02 | 56.41 | 10.52 | 0.52 | 2.30 |
| F3 | 64.76 | 26.93 | 7.35 | 0.05 | 0.83 |
| F4 | 40.92 | 52.89 | 4.03 | 0.45 | 1.71 |
| F5 | 73.71 | 23.14 | 2.15 | 0.41 | 0.61 |
| F6 | 78.62 | 18.34 | 1.97 | 0.24 | 0.54 |
| F7 | 85.94 | 7.99 | 5.72 | 0.05 | 0.03 |
| F8 | 44.68 | 49.73 | 4.23 | 0.35 | 1.02 |

Table III. Chemical composition (wt. %) of Fig. 7.

| | Fe | Cr | W | V | Mo |
|---|---|---|---|---|---|
| F22 | 25.81 | 66.20 | 5.06 | 0.66 | 2.28 |
| F23 | 25.22 | 64.87 | 7.14 | 0.57 | 2.06 |
| F24 | 23.86 | 68.45 | 5.79 | 0.35 | 1.57 |
| F25 | 25.50 | 65.90 | 8.11 | 0.48 | 0.00 |
| F26 | 92.29 | 6.72 | 0.81 | 0.15 | 0.00 |
| F27 | 89.02 | 7.25 | 3.13 | 0.26 | 0.28 |

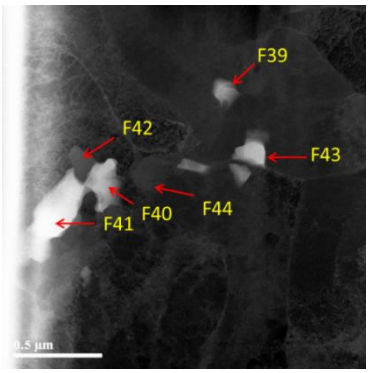


Fig. 9. TEM image of cross-section of Ar-aged specimens after exposure to 650℃ for 1,512h [4].

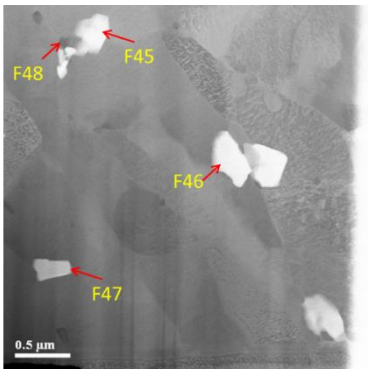


Fig. 11. TEM image of cross-section of Ar-aged specimens after exposure to 650℃ for 2,973h [4].

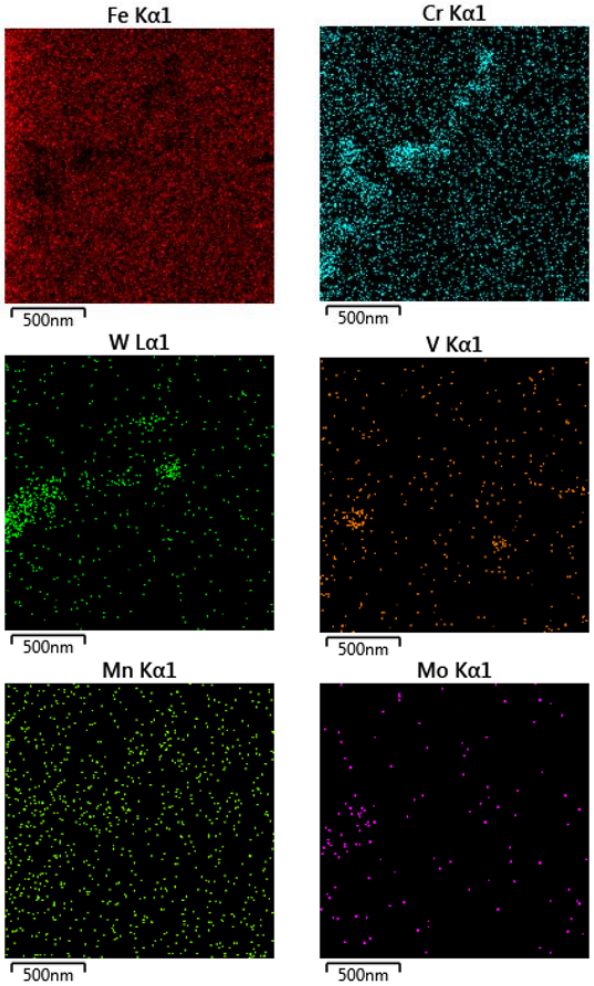


Fig. 10. EDS mapping of cross-section of Ar-aged specimens after exposure to 650°C for 1,512h shown in Fig. 9 [4].

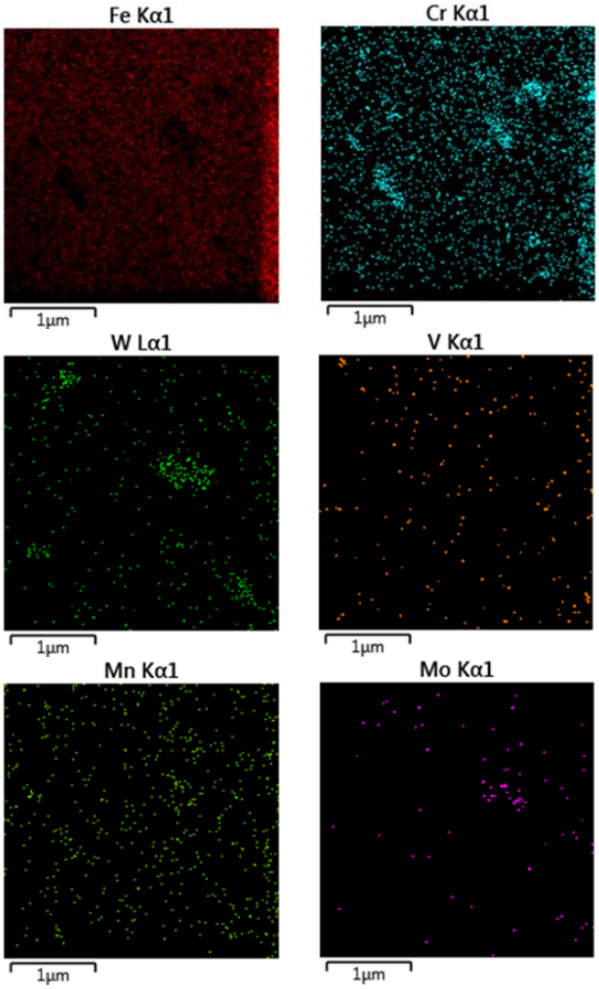


Fig. 12. EDS mapping of cross-section of Ar-aged specimens after exposure to 650°C for 2,973h shown in Fig. 11 [4].

Table IV. Chemical composition (wt. %) of Fig. 9.

| | Fe | Cr | W | V | Mn | Mo |
|---|---|---|---|---|---|---|
| F39 | 69.62 | 10.26 | 15.28 | 0.00 | 0.31 | 4.63 |
| F40 | 67.37 | 10.11 | 17.03 | 0.03 | 0.75 | 5.38 |
| F41 | 58.35 | 10.79 | 24.72 | 0.13 | 0.34 | 5.96 |
| F42 | 58.78 | 10.78 | 23.38 | 0.06 | 0.38 | 6.98 |
| F43 | 90.12 | 8.76 | 0.72 | 0.07 | 0.07 | 0.00 |
| F44 | 90.05 | 9.15 | 0.49 | 0.00 | 0.28 | 0.28 |

Table V. Chemical composition (wt. %) of Fig. 11.

| | Fe | Cr | W | V | Mo |
|---|---|---|---|---|---|
| F45 | 63.34 | 9.59 | 21.34 | 0.00 | 5.43 |
| F46 | 51.64 | 10.09 | 30.11 | 0.00 | 8.18 |
| F47 | 52.12 | 9.88 | 31.49 | 0.10 | 6.43 |
| F48 | 84.12 | 8.20 | 6.10 | 0.20 | 1.17 |

Cr was depleted from inner surface into liquid sodium, was diffused to form $NaCrO_2$ at under the surface or aggregated into grain boundary to precipitate, such as $M_{23}C_6$ [4]. Therefore, precipitates, such as laves-phase and M23C6, shown in Figs. 5 and 7 can be formed in Cr and C depletion area. Fig. 9 and 11 show the precipitates can be formed within Gr. 92; non-depletion of Cr and C. While distribution of Cr atoms at Fig. 5 and Fig. 7 is scattered with a small quantity, the Cr atoms which are congregated like F22, F23, F24 and F25 at Fig. 7, compose $M_{23}C_6$. Nowadays, it is known that Laves-phases grow near $M_{23}C_6$ after $M_{23}C_6$ grow first [3]. So, Laves-phase is observed near $M_{23}C_6$ from Fig. 5. Nevertheless, it is hard to find many Laves-phase, because $M_{23}C_6$ is locally placed. By calculating sensitivity of precipitate formation as functions of Cr-content and C-content using JMatPro8.0, Laves-phase can be nucleated with threshold Cr level between 5 wt. % and 6 wt. % of Cr [4]. If there is Cr over 5 wt. % and 6 wt. %, formation of $M_{23}C_6$ precipitates is always accompanied. This means that Laves-phase can nucleate when there are $M_{23}C_6$ precipitates. Actually, nucleation of Laves-phase have note direct relation with Cr-content. However, the amount of Cr is important that Cr can affect formation of $M_{23}C_6$ and $M_{23}C_6$ affect Si diffusion that nucleates Laves-phase. Also, the amount of $M_{23}C_6$ precipitates decreases as C-content decreases. Therefore inner-surface exposed in sodium with depletion of Cr and C, there are a few of $M_{23}C_6$. Moreover Laves-phase is hard to nucleate.

Comparing precipitates in the matrix exposed to liquid sodium with those exposed in Ar-gas, distributions of Cr atoms, which is in the matrix of the specimen treated in Ar-gas environment (Figs. 9 and 10), are more evenly scattered with more amounts than at sodium aging. And then, the number of Laves-phase in Fig. 9 is more than in Figs. 5 and 7. At Fig. 9, distributions of tungsten atoms, which compose Laves-phase, coexist with distributions of Cr atoms. It seems that there is propensity that Laves-phase can be formed near $M_{23}C_6$. Although concentrations of W and Mo are also important for Laves-phase, the solubility of W and Mo in ferrite interphase is low and diffusivity of them is higher than Si [5]. Because oversize atom like Cr, W and Mo can weakly bond with interstitial site, they are depleted at sink [3]. Therefore enough W and Mo are segregated into grain boundary to nucleate Laves-phase. Instead of them, Nucleation of Laves-phase is determined by concentration of Si segregation since diffusion of Si is slow. For the stability of Laves phase, a lot of Si is required [6]. However, concentration of Si in ferrite is different from $M_{23}C_6$. This results in differ growth rate between Ar-gas-environment and liquid sodium environment. Laves-phase is affected by Si concentrations [6]. The growth rate is calculated with below equations [6].

$$\frac{dR}{dt} = K_s * \frac{\sqrt{D_{Si}^{\alpha}}}{\sqrt{t}} \quad (1)$$

$$K_s = \frac{R(t)-R(0)}{\sqrt{4D_{Si}^{\alpha} * t}} \quad (2)$$

$$2K_s^2[1 - \sqrt{\pi}K_s * \exp(K_s^2) * erfc(K_s)] = S \quad (3)$$

$$S = \frac{c_x - c_\infty}{c_x - c_L} \quad (4)$$

, where dR/dt is growth rate of Laves-phase, $K_s$ is thermodynamic constant, $D_{Si}$ is diffusion coefficient of Si. $c_{\alpha/L}$ represents the Si concentrations in the α -ferrite side near the interface between Laves-phase and α -ferrite. $c_{M23C6}$ represents the Si concentration in the $_{M223-C6)}$. $c_L$ represents the Si concentration in the Laves-phase side. $c_\infty$ represents the Si concentration in center of the α –ferrite. $S_{M23C6}$ represents a ratio of Si concentration gradient between from α –ferrite to $M_{23}C_6$ and from Laves-phase to $M_{23}C_6$. $S_{\alpha/L}$ represents a ratio of Si concentration gradient between from α –ferrite to Laves-phase and from Laves-phase to α –ferrite. $K_{M23C6}$ and $K_{\alpha/L}$ are calculated values from equation (3) using $S_{M23C6/L}$ and $S_{\alpha/L}$.

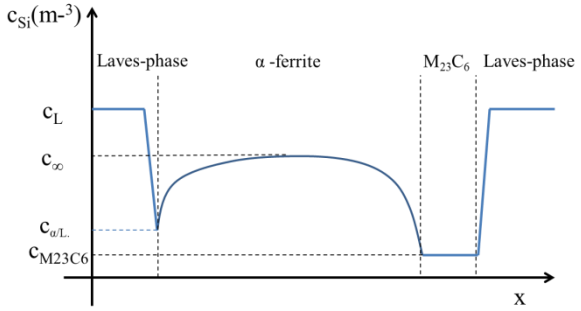


Fig. 13. The Si concentration profile in Laves phase - α ferrite - $M_{23}C_6$ - Laves phase.

$S_{M23C6/L}$ is larger than $S_{\alpha/L}$, since $c_{M23C6/L}$ is smaller than $c_{\alpha/L}$. In other words, when there are many $M_{23}C_6$ near a grain boundary, diffusivity of Si toward grain boundary increases. As for equation, $K_{M23C6/L}$ is larger than $K_{\alpha/L}$ from equation (3). Given time, dR/dt near $M_{23}C_6$ is larger. This means that more Laves-phase can nucleate and grow at Ar-gas environment in which there is more $M_{23}C_6$, due to more effect of Si stability for Laves-phase.

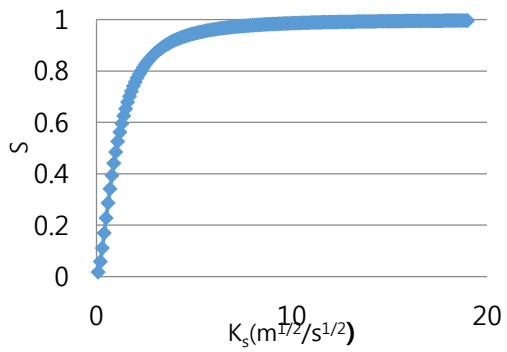


Fig. 14. Plot of eq. (3)

To understand the thermodynamic reasons for formation of $M_{23}C_6$ and Laves-phase, Gibbs free energy is calculated with below equations [7].

$$\Delta G^{\circ}_{T} = \Delta H^{\circ}_{T} - T\Delta S^{\circ}_{T} \quad (5)$$

$$\Delta H^{\circ}_{T} = \Delta H^{\circ}_{298,T} + \int_{298}^{T} \Delta C^{\circ}_{P} dT \quad (6)$$

$$\Delta S^{\circ}_{T} = \Delta S^{\circ}_{298,T} + \int_{298}^{T} \left(\frac{\Delta C^{\circ}_{P}}{T}\right) dT \quad (7)$$

Gibbs free energies of main precipitates about aged at 650℃ are summarized in Table VI.

Since $M_{23}C_6$ has low Gibbs free energy, the tendency of formation of $M_{23}C_6$ has high possibility. Accordingly, Cr atoms gather together due to formation of Cr precipitates like Fig. 5, 7, 9 and 11. However, all precipitates including Cr atom don't mean $M_{23}C_6$.

It is also possible to precipitate MX or $MX_2$ which has comparatively low Gibbs free energy, since there are many surplus Cr and C atoms

Table VI. Gibbs free energy of Precipitates at 650℃ [8].

| Precipitate | ΔG(kJ/mol) |
|---|---|
| $Cr_{16}Fe_6C_6$ ($M_{23}C_6$) | -678.111 |
| $Cr_4Fe_{12}Mo_4Si_2WVC_6$ ($M_{23}C_6$) | -775.594 |
| CrVNbN (Z-phase) | -242.755 |
| $V_4C_3$ (Vanadium) | -153.273 |
| $Fe_2Mo$ (Laves-phase) | -94.8773 |
| $Fe_2W$ (Laves-phase) | -98.1707 |
| $Fe_2$(Mo, W) (Laves-phase) | -130.156 |
| NbN (MX) | -194.753 |
| VN (MX) | -188.209 |
| (CrV)N (MX) | -218.405 |
| Nb(CN) (MX) | -203.351 |
| $Mo_2C$ ($M_2X$) | -213.26 |

Comparing sub-grain size of matrix exposed to sodium with those exposed to Ar-gas environment, Grain boundary density at Ar-aging is about twice than at sodium environment. This means that there are small grain size and high grain boundary angle at Ar-gas environment. The reason can be founded at formation of precipitates.

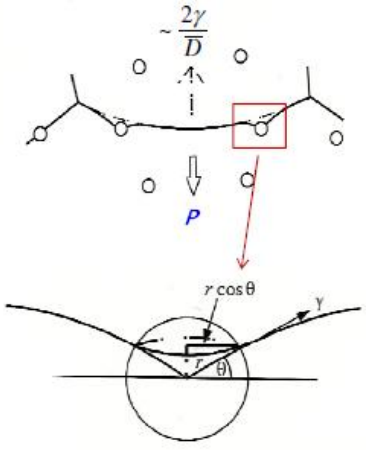


Fig. 15. The effect of spherical particles on grain boundary migration [9]

Table VII. Grain boundary density of specimens (#/μm)

| Na-1583h | Na-3095h | Ar-1512h | Ar-2973h |
|---|---|---|---|
| 1.52 | 1.75 | 3 | 3.46 |

Effect of precipitate on grain growth during thermal aging can't be negligible. Grain size is related with below equations.

$$F = \pi r\gamma * sin2\theta \leq \pi r\gamma = F_{max} \quad (8)$$

$$N_s = \frac{3f}{2\pi r^2} \quad (9)$$

$$P_{max} = F_{max} * N_s = \frac{3f\gamma}{2r} \quad (10)$$

, where $F$ is force exerted by a precipitate at grain boundary, $N_s$ is the number of precipitate per unit area, P is pressure exerted b precipitate at grain boundary, $f$ is volume fraction of precipitate and $r$ is radius of a precipitate. And grain growth occurs when

$$P_{max} < \frac{2\gamma}{D} \quad (11)$$

$$D_{max} \propto \frac{r}{f} \quad (12)$$

, where D is grain size. Therefore maximum grain size is proportional to radius of a precipitates and inverse proportional to volume fraction of precipitates. At sodium environment, there is low volume fraction of precipitates due to leakage of Cr and C. Therefore grain boundary density can be expected by effect of precipitates on grain growth.

## 4. Conclusions

When Gr.92 is exposed to sodium containing oxygen, oxide is formed and there are depletion of Cr and presumably decarburization into sodium. So, the amount of $M_{23}C_6$ is decreased. At Ar-gas environment, there is no depletion of Cr and C. So, $M_{23}C_6$ and Laves-phase are normally observed. Laves-phase can be formed easily when there are many $M_{23}C_6$, because the precipitates increase diffusivity of Si which make Laves-phase stabilized. Therefore, Laves-phase can be observed at Ar-gas environment in which there are many $M_{23}C_6$.. This behavior of precipitates can affect grain growth by pinning effect. Therefore, small grains at Ar-gas environment are more to be affected by pinning effect. On the other hand, large grains are observed at sodium environment aging which have small volume fraction of precipitates.

## REFERENCES

[1] S.H. Shin, J.J. Kim, J.A. Jung, K.J. Choi and J.H. Kim Development of experimental system for materials compatibility test for ultra-long cycle fast reactor (UCFR), NFSM, American Nuclear Society, 2012, Chicago, IL.
[2] J.A. Jung, S.H. Kim, S.H. Shin, I.C. Bang and J.H. Kim, Feasibility study of fuel cladding performance for application

in ultra-long cycle fast reactor, Journal of Nuclear Materials, Vol. 440, p. 596-605, 2013.
[3] R. L. Klueh and D. R. Harries, High-chromium ferritic and martensitic steels for nuclear applications, ASTM Int'l, 2012.
[4] S.H. Shin, J.H. Kim and J.H. Kim, Effect of Aging ASTM A182 Grade 92 Steel on Corrosion Behavior and Microstructural evolution in Liquid Sodium at 650°C, under Review, Corrosion science, Vol.97, p.172-182, 2015
[5] M.I. Isik, A. Kostka, V.A. Yardley, K.G. Pradeep, M.J. Duarte, P.P. Choi, D. Raabe and G. Eggeler, The nucleation of Mo-rich Laves phase particles adjacent to $M_{23}C_6$ micrograin boundary carbides in 12% Cr tempered martensite ferritic steels, Acta Materialia Vol.90, p.94-104, 2015
[6] A. Aghajani, F. Richter, C. Somsen, S.G. Fries, I. Steinbach and G. Eggeler, On the formation and growth of Mo-rich Laves phase particles during long-term creep of a 12% chromium tempered martensite ferritic steel, Scripta Materialia, Vol.61, p.1068-1071, 2009.
[7] D. V. Ragone, Thermodynamics of Materials-Volume I, Wiley, p. 127-130, 1994.
[8] M. Winter, The university of Sheffield and WebElement Ltd , UK, 1993.
[9] D. A. Porter et al., Phase transformations in metals and alloys – third edition, p. 145, 2009